https://doi.org/10.55453/rjmm.2025.128.4.2

ORIGINAL ARTICLE

Exploring Gliosarcoma by Light Microscopy, Two-Photon Excitation Microscopy, and Radiological Imaging Techniques

Adrian Enache[1,2,3], Lucian G. Eftimie[1,2,4], Radu Hristu[1], Remus R. Glogojeanu[4], Mircea Bratu[4], Oana C. Voinea[3], Maria Sajin[3], George A. Stanciu[1], Octavian M. Sîrbu[2,3]

[1] Center for Microscopy-Microanalysis and Information Processing, National University of Science and Technology Politehnica Bucharest, Romania lucicaeftimie@yahoo.com, radu.hristu@upb.ro, adrianenache20@yahoo.com, stanciu@physics.pub.ro

[2] "Dr. Carol Davila" Central Military Emergency University Hospital Bucharest, Romania adrianenache20@yahoo.com, lucicaeftimie@yahoo.com, octavian.mihai-sirbu@drd.umfcd.ro

[3] "Carol Davila" University of Medicine and Pharmacy, Bucharest, Romania octavian.mihai-sirbu@drd.umfcd.ro, adrianenache20@yahoo.com, oanacristinavoinea@gmail.com, maria_sajin@yahoo.com

[4] Department of Special Motricity and Medical Recovery, The National University of Physical Education and Sports, Bucharest, Romania remusglogo@gmail.com, mircea.bratu@yahoo.com, lucicaeftimie@yahoo.com

Correspondence: Lucian G Eftimie, lucicaeftimie@yahoo.com; Remus R Glogojanu, remusglogo@gmail.com

Abstract: Gliosarcoma is a rare and aggressive variant of glioblastoma, characterized by both a malignant glial component and a mesenchymal sarcomatous component. Gliosarcomas have genetic alterations with glioblastomas, including TP53, PTEN mutations, and EGFR amplification, but may also exhibit additional changes related to epithelial-mesenchymal transition pathways. Management is similar to glioblastoma, involving safe, maximal surgical resection followed by radiotherapy and chemotherapy with temozolomide, but the prognosis remains poor, with a median survival of 6-14 months. Both Magnetic Resonance Imaging (MRI) and Computed Tomography (CT) play crucial roles in the detection, characterization, and treatment planning of gliosarcoma. While MRI is the gold standard, CT remains valuable in certain situations. Light microscopy is essential for definitive diagnosis, allowing pathologists to examine cellular morphology and tissue architecture. It is essential for distinguishing gliosarcoma from other high-grade gliomas and for guiding treatment decisions. In addition, two-photon excited fluorescence (TPEF) microscopy is an advanced optical imaging technique that enables real-time, high-resolution visualization of tumor tissue without the need for staining or contrast agents and enhances visualization of collagen structure and vascularization, key factors in gliosarcoma assessment. The study of radiological and histopathological (light microscopy) features in primary gliosarcomas of the brain is a priority to achieve an early diagnosis that can be translated into better outcomes. Here, we describe the radiological and histopathological features observed in multiple cases of gliosarcoma in current practice.

Keywords: gliosarcoma; histopathology; light microscopy; two-photon excited fluorescence; radiology; magnetic resonance imaging; neurosurgery

INTRODUCTION

Gliosarcoma is a rare and highly malignant primary neoplasm of the central nervous system (CNS), classified as WHO grade 4. It is characterized by a biphasic histopathological pattern, comprising both glial and mesenchymal components. The peak incidence occurs around the sixth decade of life, with a male-to-female ratio of 1.8:1 [1,2,3]. While most cases are primary, secondary gliosarcomas may develop in patients with previously resected glioblastomas or as a consequence of cranial irradiation. Clinically, gliosarcoma often presents with symptoms such as headache, seizures, and hemiparesis. Due to their aggressive nature, tumors are typically large at diagnosis and frequently cause midline shift [4,5], particularly in the temporal lobe, as revealed by computed tomography (CT) and magnetic resonance imaging (MRI).

Brain and other nervous system malignancies constitute a significant proportion of cancer-related deaths, particularly among children and young adults [6]. Gliomas, the most common primary brain tumors in adults, originate from glial cells and are highly invasive, diffusely infiltrating the surrounding brain parenchyma. Glioblastoma multiforme (GBM), the most aggressive glioma subtype, has a particularly poor prognosis, with a median survival of less than one year and a five-

Citation: Enache A, Eftimie LG, Hristu R, Glogojeanu RR, Bratu M, Voinea OC, Sajin M, Stanciu GA, Sîrbu OM. *Exploring Gliosarcoma by Light Microscopy, Two-Photon Excitation Microscopy, and Radiological Imaging Techniques*. R. J. Mil. Med. 2025, 128(4): 276-285; https://doi.org/10.55453/rjmm.2025.128.4.2

Academic Editor: Clara Ursescu

Received: 15 February 2025
Revised: 28 April 2025
Accepted: 8 May 2025

year survival rate below 5% [7,8]. The dismal survival outcomes are attributed to the tumor's extensive infiltration, limiting the effectiveness of surgical resection, and leading to inevitable recurrence.

Preoperative imaging modalities such as MRI, CT, single-photon emission computed tomography (SPECT), and positron emission tomography (PET) provide critical insights into tumor localization and characteristics [9]. However, intraoperative identification of residual tumor tissue remains a major challenge. The extent of surgical resection is a key determinant of overall survival and progression-free survival in glioma patients. Achieving maximal safe resection necessitates advanced intraoperative imaging techniques [10] to differentiate tumor tissue from normal brain structures with high specificity and sensitivity.

Recent advances in molecular biology have significantly improved the classification and diagnosis of brain tumors. The integration of molecular markers has refined tumor characterization, enabling more precise prognostic assessments [11]. However, the routine implementation of molecular testing is limited by accessibility constraints, particularly in resource-limited settings [12,13,14]. Furthermore, molecular data interpretation can be complex, and in certain cases, tumors are categorized as "not otherwise specified" (NOS) when genetic features are ambiguous or unavailable.

Histopathological evaluation remains a cornerstone in brain tumor diagnosis [15], with light microscopy providing critical insights into cellular morphology, mitotic activity, necrosis, and vascular proliferation. Hematoxylin and eosin (H&E) staining, alongside immunohistochemical markers, enhances tumor characterization. Despite its essential role, conventional light microscopy alone may not always provide sufficient contrast for distinguishing malignant from benign or reactive tissues. Consequently, there is growing interest in complementary optical imaging techniques for improved tumor assessment.

Emerging optical imaging modalities, including confocal microscopy and nonlinear optical (NLO) microscopy [16,17,18], offer promising non-invasive diagnostic capabilities. Among these, two-photon excited fluorescence (TPEF) microscopy [19] has gained attention due to its ability to generate high-resolution images of biological tissues with minimal photodamage [20,21,22]. TPEF operates by simultaneously absorbing two lower-energy photons, exciting endogenous or exogenous fluorophores, and producing a fluorescence signal. This technique enables detailed visualization of cellular and extracellular structures, making it a valuable tool for characterizing brain tumors, including gliosarcomas.

Most studies utilizing TPEF microscopy in brain tumor research have relied on exogenous fluorescent dyes or genetically expressed fluorescent proteins [23] to achieve image contrast for visualizing tumor cells, neurons, and blood vessels [24,25,26]. However, intrinsic fluorescence signals from endogenous biomolecules [27], such as nicotinamide adenine dinucleotide (NADH) and flavin adenine dinucleotide (FAD), can also be leveraged for label-free tumor imaging. TPEF microscopy has demonstrated significant potential in various biomedical applications, including neurobiology [28], tissue engineering [29], and in vivo optical biopsies [30], highlighting its versatility in tumor diagnostics.

In this study, we explore the potential of TPEF microscopy as a complementary imaging tool for gliosarcoma diagnosis, alongside conventional modalities such as CT, MRI, and histopathology. By leveraging TPEF's high-resolution and label-free imaging capabilities, we aim to enhance the visualization of gliosarcoma-specific features, ultimately contributing to improved tumor identification and diagnostic precision.

MATERIALS AND METHODS

These cases were retrieved from the files of our department. In the past 9 years (2016-2024), the department's archive contained and diagnosed 10 cases of gliosarcoma. From these cases, we obtained MRI and CT images for illustration, which we compared with images acquired from tissue sections embedded in paraffin.

The tissue was fixed in a 10% buffered formalin and embedded in paraffin, with 4-5 microns-thick paraffin sections. On hematoxylin-eosin (HE) stained sections, the glial component showed malignant astrocytes, with associated microvascular proliferation and geographic necrosis, while the sarcomatous components showed pleomorphic spindle cells. Features identified on CT and MRI scans were partial uptake of contrast agent with a ring-enhancement pattern, peripheral edema, and central calcification. The tumor displayed a specific pattern in TPEF imaging. Selected regions of interest were examined using a Leica TCS SP laser scanning confocal microscope optimized for nonlinear imaging. The excitation source was a Ti: Sapphire laser (Coherent Chameleon Ultra II) tuned to 860 nm, with a pulse width of 140 fs and a repetition rate of 80 MHz. During scanning, the laser power at the objective focus was kept below 10 mW. A 10× objective (NA 0.3) was used to focus the excitation beam onto the samples and collect the TPEF signal in epi-detection. The resulting field of view was 1 × 1 mm^2. Spectrally resolved detection, inherent to the Leica TCS SP system, was used to capture TPEF signals in the 450–700 nm range. Also, the distinction between tumor and peritumoral brain zone was easy in TPEF analysis, allowing a clear visualization of the brain/tumor interface. TPEF imaging is a fast and efficient method allowing analysis of brain tumor tissue.

RESULTS

MRI and CT analysis

The images were obtained in our hospital, and the MRI characteristics were evaluated. Gliosarcomas can be very similar to glioblastomas in appearance. These are usually widely localized peripheral lesions with possible direct dural invasion or only reactive dural thickening (dural tail). On MRI, gliosarcomas typically present as heterogeneously enhancing lesions with irregular margins,

often associated with significant peritumoral edema and central necrosis. They may also demonstrate areas of hemorrhage and variable diffusion restriction. The tumor frequently involves the cerebral hemispheres, with a predilection for the temporal and frontal lobes.

Figure 1: MRI images demonstrating a gliosarcoma with typical localization in the left temporal lobe – A) Sagittal section in T1-weighted imaging; B) Axial section in T2-weighted imaging; C) Coronal section in Fluid Attenuated Inversion Recovery (FLAIR) sequence; D) Sagittal section in post-contrast T1-weighted imaging; E-F) Maximum Intensity Projection (MIP) reconstruction; G) Diffusion-weighted imaging in axial plane; H) Apparent Diffusion Coefficient (ADC) in axial plane; I) Axial section in Susceptibility Weighted Imaging (DWI) sequence

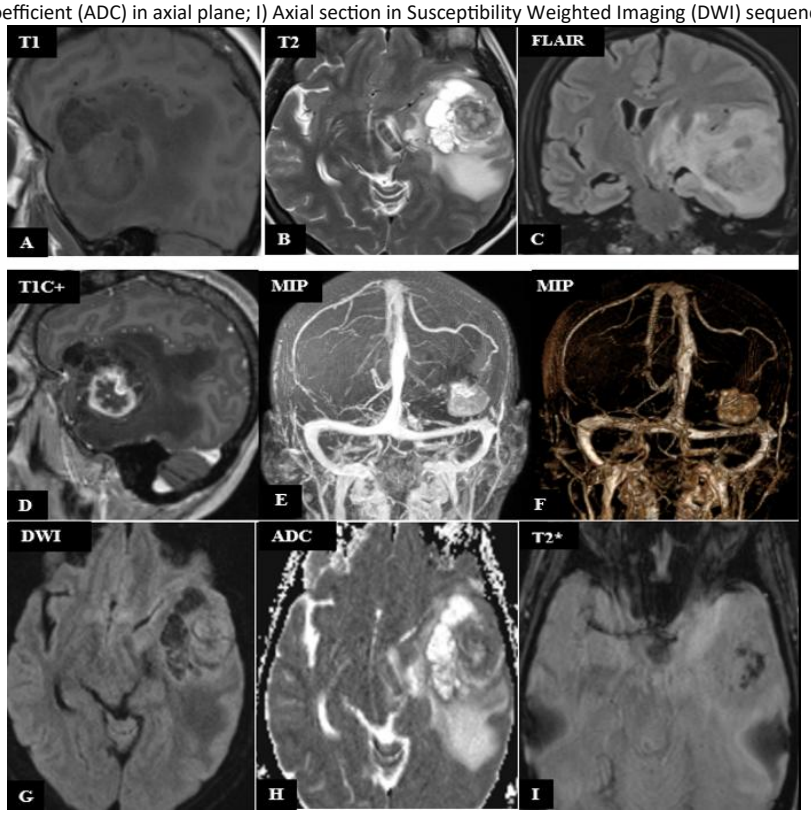

Figure 2: MRI image with postoperative appearance 4 days after surgery - No tumor debris - A) Sagittal section in T1-weighted imaging; B) Axial section in T2-weighted imaging; C) Sagittal section in post-contrast T1-weighted imaging; D) Axial section in subtraction imaging between native T1 and post-contrast T1; E) Diffusion-weighted imaging in axial plane; F) Apparent Diffusion Coefficient (ADC) in axial plane

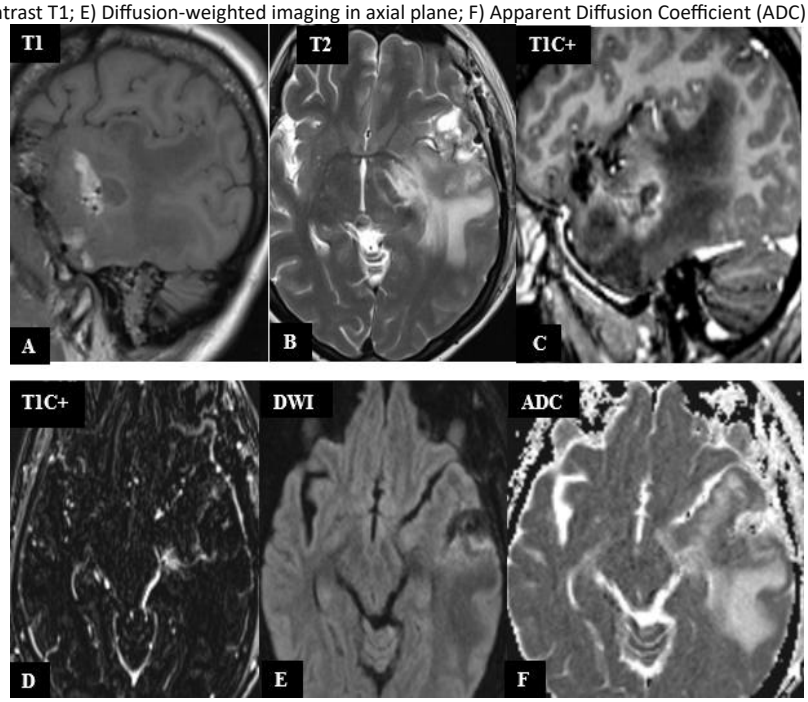

As can be observed in Figure 1, MRI confirms an intra-axial mass in the left temporal lobe. The lesion demonstrates a heterogeneous pattern of central hypersignal and marginal hyposignal on T1-weighted images (Figure 1A) and peripheral hypersignal with central hyposignal on T2-weighted images (Figure 1B), which is consistent with a solid-cystic mass. We can see the ring-enhancement pattern on T1-weighted Gadolinium images (Figure 1D) with central necrosis, as seen in DWI and ADC sequences (Figures 1G-H). A great amount of perilesional edema can be noticed on FLAIR images (Figure 1C). The high vascularity and intratumoral neo-vascularization can be observed on angio-MRI reconstructed images (Figures 1E-F). Small areas of intratumoral hemorrhage can be noted on T2*-weighted images (Figure 1).

In Figure 2, we have MRI images with postoperative appearance 4 days after surgery, with the presence of a marginal contrast-enhanced (Figure 2C, D), left temporal post-interventional porencephalic cavity (Figure 2A, B). No tumor debris present or diffusion restrictions in the surgical area were identified (Figure 2E, F).

MRI images of postoperative appearance 6 days after surgery showed postoperative left temporal changes with a slight decrease in the porencephalic cavity compared to the previous examination (Figure 3). Significant reduction of cerebral edema. On the MIP reconstructions performed from the T1 subtraction sequence with contrast, the disappearance of the tumor seen in Figure 1 is observed (Figure 3F).

Figure 3: MRI images of postoperative appearance 6 days after surgery - No tumor debris present - A) Sagittal section in T1-weighted imaging; B) Axial section in T2-weighted imaging; C) Coronal section in Fluid Attenuated Inversion Recovery (FLAIR) sequence; D) Axial section in post-contrast T1-weighted imaging; E) Coronal section in post-contrast T1-weighted imaging; F) Maximum Intensity Projection (MIP) reconstruction; G) Diffusion-weighted imaging in axial plane; H) Apparent Diffusion Coefficient (ADC) in axial plane; I) Axial section in Susceptibility Weighted Imaging (SWI) sequence

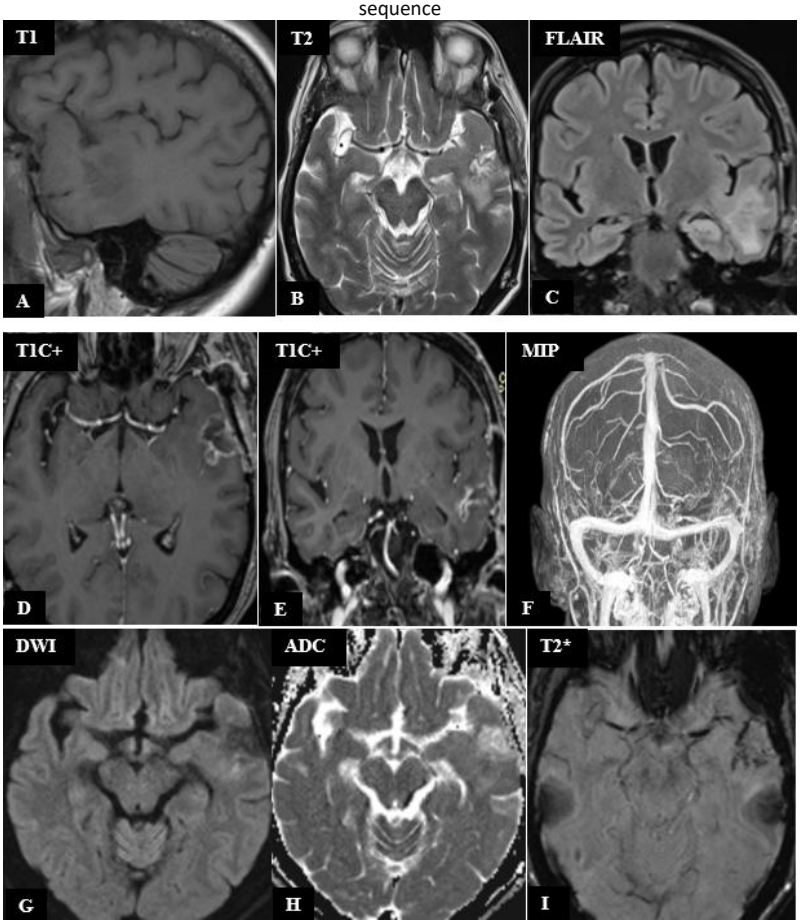

Unfortunately, after 4 months postoperatively, the patient presented again to the emergency department, and he had a head CT scan (Figure 4). The diagnosis was tumor recurrence, which causes mass effect (Figure 4A, C), peritumoral edema (Figure 4A, B, C), displacement of midline shift due to tumor and edema (Figure 4A, C) and herniation of the left contralateral cerebral parenchyma with a subfalcine herniation appearance (Figure 4C).

Gliosarcomas, like glioblastomas, exhibit a high recurrence rate, with most recurrences occurring within the first year following initial treatment. Recurrence often presents with rapid growth and can be more aggressive than the initial tumor, due to the tumor's inherent heterogeneity and resistance to therapy. The prognosis for patients with recurrent gliosarcoma is poor, with limited survival rates. The overall survival after recurrence is typically shorter than for primary tumors.

Figure 4: CT images were obtained 4 months postoperatively - tumor recurrence - A) Axial section (native); B) Sagittal section (native); C) Coronal section (native).

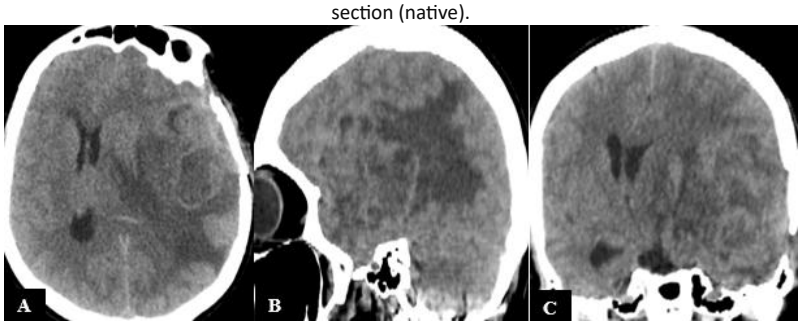

Light microscopy

Images acquired with bright-field microscopy on H&E-stained tissue sections highlight the aspects of a gliosarcoma, which exhibits a biphasic histological pattern, with alternating regions of glial and mesenchymal differentiation. The glial component resembles glioblastoma, characterized by atypical astrocytic cells with pleomorphic nuclei, increased mitotic activity, and areas of necrosis with pseudopalisading (Figure 5A; Figure 6B). The mesenchymal component consists of spindle-shaped cells arranged in fascicles, resembling fibrosarcoma (Figure 5B). Optical microscopy is essential for detecting vascular proliferation, a hallmark of gliosarcoma, including endothelial hyperplasia and abnormal vascular structures. This feature is significant in distinguishing gliosarcoma from other tumors (Figure 6A).

Figure 5: (A) Glial component showing large, pleomorphic, fibrillary astrocytic cells with atypical mitosis in the center (marked with an arrow). (B) Sarcomatous component showing spindle cells arranged in a pattern of densely packed, long bundles

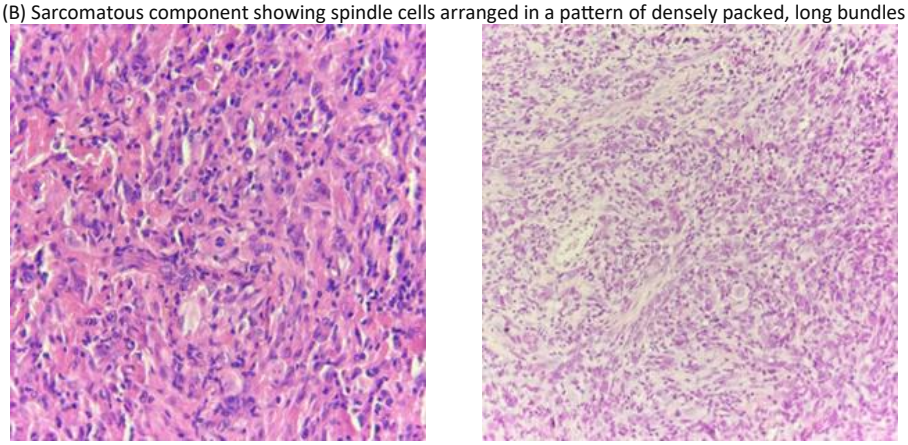

The mitotic index and cellular density observed through light microscopy are useful for grading the tumor. High mitotic activity correlates with a higher grade and a more aggressive tumor. Light microscopy can help assess the peritumoral edema and the extent of surrounding tissue invasion, giving insights into how the tumor interacts with the surrounding brain structures.

Figure 6: (A) Microvascular proliferation is represented by multilayered, small-caliber blood vessels with a glomeruloid appearance (several blood vessels marked with arrows). (B) Geographic necrosis (pseudopalisading neoplastic cells surrounding a central area of tumor necrosis), marked with an arrow

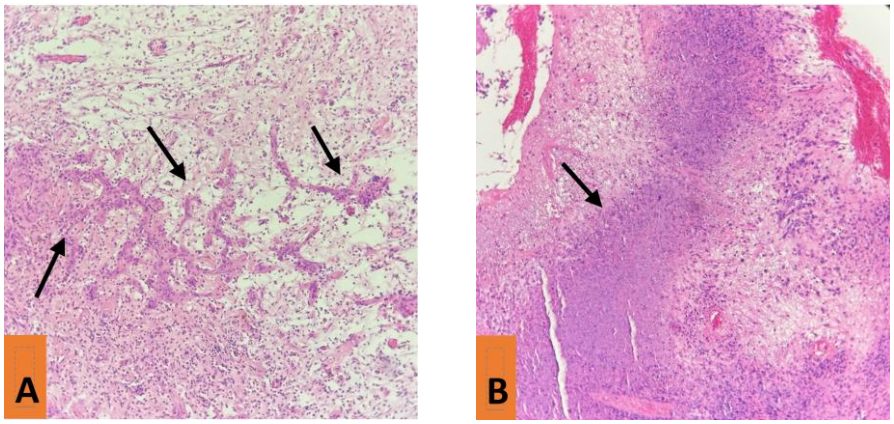

Recurrences often show similar histological features to the original tumor but may have increased cellularity, more prominent necrosis, or increased vascular proliferation.

Understanding the exact histopathological features through light microscopy assists clinicians in treatment planning, as the tumor's aggressiveness, heterogeneity, and vascular properties influence the choice of therapy (e.g., surgical resection, radiotherapy, chemotherapy).

Light microscopy compared to two-photon excited fluorescence (TPEF)

By integrating optical microscopy and TPEF, this study aims to enhance the understanding of gliosarcoma's complex microenvironment, exploring the advantages and limitations of each method in tumor characterization. Our findings provide insights into the potential of TPEF as a complementary diagnostic tool, bridging the gap between traditional histopathology and advanced optical imaging techniques.

Figure 7: (A) Light microscopy image of large, highly pleomorphic glial cells, with bizarre nuclei, mitotic activity in the center (arrow), and microvascular proliferation on the right (asterisk) with corresponding TPEF image – Figure 7 (B).

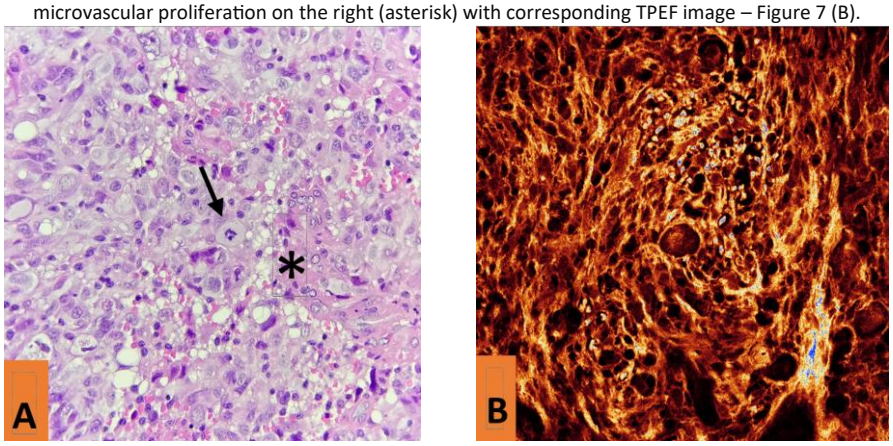

Figure 8: (A) Light microscopy image showing a biphasic pattern, represented by atypical, glial cells intermingled with spindle, sarcomatous cells. (B) Corresponding TPEF microscopy showing the corresponding image

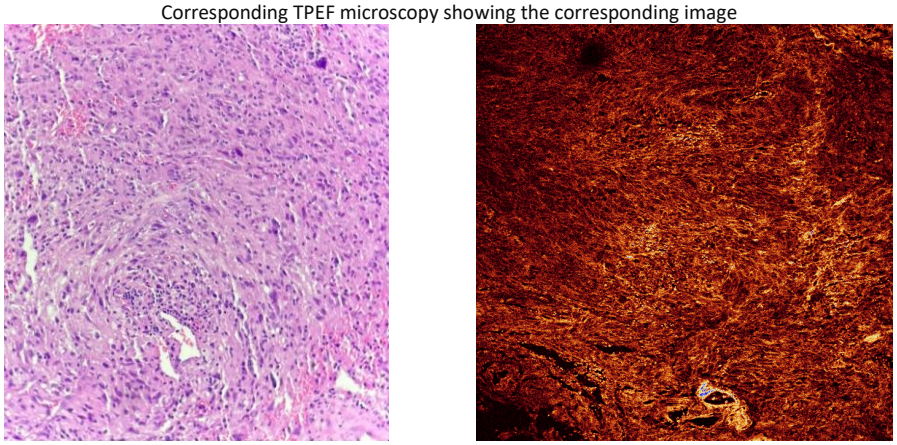

As can be observed in Figures 7 and 8, the pleomorphic nature of cells in gliosarcoma is one of the most striking features observed under light microscopy and TPEF. The glial component of the tumor typically consists of atypical astrocytic cells with varying sizes, shapes, and nuclear characteristics, which include prominent nucleoli, irregular nuclear contours, and increased mitotic figures (Figure 7A). This cellular pleomorphism reflects the aggressive nature of the tumor and contributes to its histopathological diagnosis as a high-grade glioma. In contrast, the mesenchymal component of gliosarcoma exhibits spindle-shaped cells with less defined borders, further adding to the pleomorphic architecture of the tumor (Figure 8A).

In Two-Photon Excitation Fluorescence (TPEF) imaging, the pleomorphic cellular structure is also identifiable, but through label-free imaging that highlights differences in tissue architecture based on endogenous fluorescence. While TPEF cannot provide the same cellular details as optical microscopy, it offers insights into the variations in cellular and extracellular matrix composition that correspond to the pleomorphic nature of gliosarcoma cells. The increased autofluorescence in areas with high cellularity and metabolic activity, as seen in the glial component (Figure 7B), contrasts with the more fibrous and structured mesenchymal regions, providing a complementary visualization of the tumor's heterogeneity (Figure 8B). TPEF's ability to image deep tissue also offers a broader view of how pleomorphic regions interact with surrounding structures, complementing the histopathological observations made under optical microscopy.

Figure 9: (A) Light microscopy image showing a vessel-rich, fibrosarcomatous area of the tumor, composed of spindle cells, with (B) the corresponding TPEF microscopy image

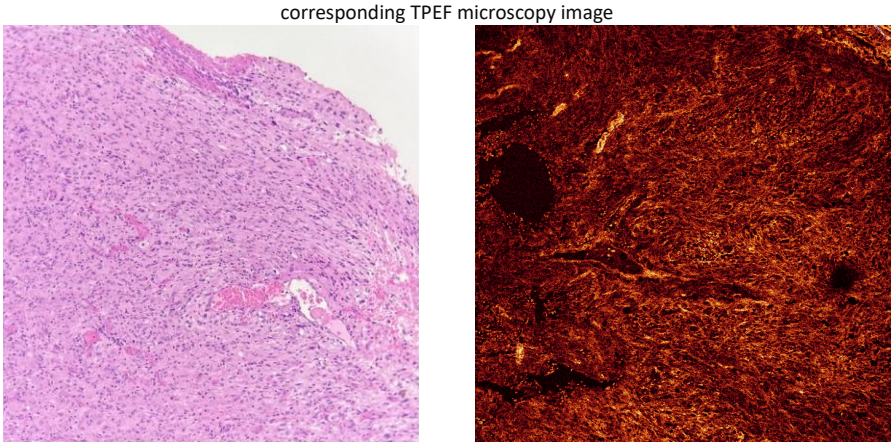

Under light microscopy, these vascular changes are readily observed, particularly the presence of abnormal, hyperplastic blood vessels that often exhibit endothelial cell proliferation and vascular lumen formation. These blood vessels may appear as tortuous and irregular in shape, contributing to the high degree of neovascularization characteristic of high-grade gliomas (Figure 9A and Figure 10A). In TPEF imaging, the vascularization in gliosarcoma is also detectable, albeit in a more indirect manner. While TPEF does not specifically stain blood vessels, the increased autofluorescence in regions of high vascularity can reveal the areas where blood vessels are more concentrated, especially in regions of new blood vessel formation and vascular leakage. TPEF imaging can also visualize the extracellular matrix surrounding the vessels, allowing for the assessment of the tumor's interaction with its vascular network (Figure 9B and Figure 10B). Furthermore, the deep-tissue penetration of TPEF offers a more comprehensive view of the tumor's vasculature, providing insights into both the microvascular architecture and the surrounding tissue environment that may not be fully captured with optical microscopy alone.

Figure 10: (A) Light microscopy image showing the gliomatous component, with foci of microvascular proliferation. (B) TPEF microscopy showing the corresponding image

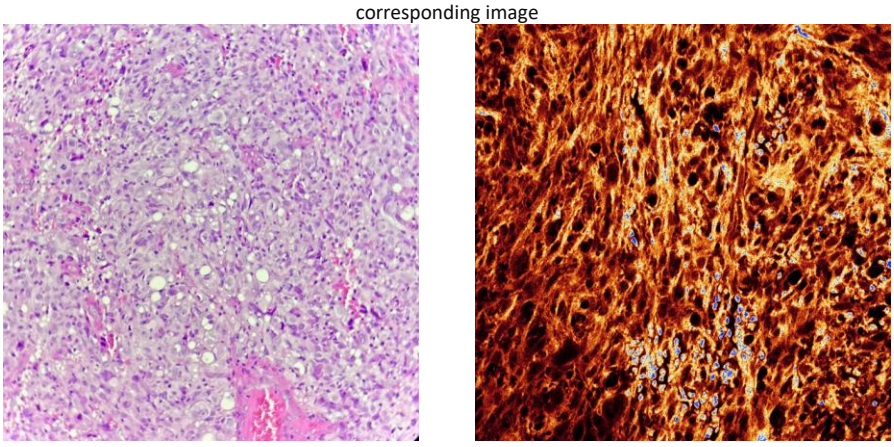

DISCUSSION

Early detection of brain tumors, including gliosarcoma, is crucial for improving treatment outcomes and patient survival. Delayed diagnosis can lead to uncontrolled tumor growth, reducing the effectiveness of therapeutic interventions. Conventional diagnostic approaches, including MRI, CT, and histopathological analysis using light microscopy, remain the gold standard for tumor identification and classification. However, these methods have inherent limitations, such as variability in manual interpretation and challenges in distinguishing tumor margins with high precision.

Light microscopy provided valuable histopathological insights into gliosarcoma, enabling the identification of distinct tumor cell characteristics and assessment of tissue architecture. However, conventional light microscopy is often complemented by immunohistochemical staining, which can introduce variability and require additional processing time. In contrast, TPEF microscopy offers a label-free, rapid, and high-resolution imaging approach for characterizing brain tumors. Our study demonstrates that TPEF microscopy effectively differentiates individual tumor cells and delineates their distribution in gliosarcoma samples.

Recent studies have explored the application of multiphoton imaging techniques in oncology. For example, TPEF microscopy has been successfully employed for brain tumor visualization, leveraging the endogenous fluorescence of metabolic coenzymes such as nicotinamide adenine dinucleotide (NADH) and flavin adenine dinucleotide (FAD) to assess cellular metabolism [31,32]. Several studies

have demonstrated the utility of metabolic imaging for distinguishing between normal and cancerous tissues [33,34]. These findings align with our results, where TPEF microscopy provided high-contrast visualization of gliosarcoma cells based on fluorescence.

Furthermore, recent advances in label-free optical imaging techniques, such as second-harmonic generation (SHG), have also been explored for brain tumor detection [35]. Compared to SHG, which primarily targets fibrillar collagen, TPEF provides direct cellular imaging, making it particularly useful for distinguishing tumor cells from surrounding neural tissue. Additionally, while confocal microscopy has been employed for intraoperative brain tumor imaging, it lacks the penetration depth and reduced photodamage advantages offered by TPEF microscopy [36].

This study introduces a novel application of TPEF microscopy for the analysis of gliosarcoma, showcasing several key advantages. Firstly, TPEF provides high-resolution with potential label-free imaging, eliminating the need for exogenous stains and thus reducing sample preparation time. The potential for intraoperative use is another strength, as real-time, high-contrast imaging of tumor margins could assist neurosurgeons in achieving maximal safe resection.

Despite these strengths, the study does have certain limitations. The analysis was performed on a limited number of gliosarcoma samples, and further validation on a larger dataset is necessary to establish robustness. Additionally, the ex vivo imaging of paraffin-embedded tissue sections, rather than fresh, in vivo samples, limits the immediate application of TPEF in clinical settings. Future studies should focus on exploring real-time, intraoperative applications of TPEF.

Looking ahead, several avenues for future research are proposed to expand the clinical applicability of TPEF microscopy. These include the integration with multimodal imaging, such as combining TPEF with SHG or Raman spectroscopy for more comprehensive tumor characterization. Further development of in vivo applications is also critical, including the creation of fiber-optic or handheld TPEF imaging systems for intraoperative brain tumor resection. Additionally, the incorporation of artificial intelligence-assisted analysis could help automate the classification of TPEF images, improving diagnostic accuracy. Finally, validation on diverse brain tumors, including glioblastoma and metastases, is essential to assess the broader diagnostic potential of TPEF microscopy.

CONCLUSION

Our study highlights the complementary roles of various imaging modalities in the comprehensive analysis of gliosarcomas. Light microscopy provides detailed insights into tissue morphology and cellular architecture, essential for initial tumor identification and classification. Two-photon excitation microscopy offers deeper tissue imaging with reduced photodamage, enabling visualization of tumor structures in their native environment. Radiological imaging techniques, such as MRI and CT scans, facilitate non-invasive assessment of tumor location, size, and progression within the brain. Integrating these methodologies enhances diagnostic accuracy and informs effective therapeutic strategies for gliosarcoma patients. When used as an additional technique with practical application in clinical settings, it may help to prevent under or overdiagnosis of certain lesions, whose accurate diagnosis is necessary for sufficient and effective treatment. Additionally, we will prevent the abuse of other currently available, somewhat expensive supplemental diagnostic methods (molecular biology techniques, genetic tests, IHC tests, electron microscopy, etc.).

Conflicts of interest and sources of funding

The authors declare no conflict of interest. No artificial intelligence automatically generated text was inserted in this manuscript, and no image was previously published in another journal or is under consideration of being published elsewhere. This research received no external funding.

Authors' contribution

Conceptualization A.E. and L.G.E.; methodology A.E., L.G.E and R.R.G..; software R.H.; validation L.G.E., R.H., O.M.S, M.S. and G.A.S.; formal analysis M.B. and O.C.V; investigation A.E.; resources L.G.E. and O.C.V.; data curation R.R.G.; writing—original draft preparation A.E.; writing—review and editing L.G.E, R.H., O.M.S. and G.A.S.; visualization R.R.G, M.B. and O.C.V.; supervision O.M.S., M.S. and G.A.S.; project administration A.E..; funding acquisition L.G.E, and R.H. All authors have read and agreed to the published version of the manuscript elaboration

Ethics approval and consent to participate

The study was conducted under the Declaration of Helsinki. The approval of the Local Ethical Committee was obtained under the number 392/9G /2025. The research was conducted under ethical guidelines and regulations, ensuring compliance with all necessary protocols. Before the study, the committee reviewed and approved the methodology, including data collection and analysis procedures, to guarantee ethical standards were met. Additionally, all patient data used in the study were anonymized to maintain confidentiality and adhere to ethical principles.

Patient consent for publication

Informed consent was obtained from all subjects involved in the study.

References:

1. Kozak K, Mahadevan A, Moody J. Adult Gliosarcoma: Epidemiology, Natural History, and Factors Associated with Outcome. Neuro Oncol. 2009;11(2):183-91. doi:10.1215/15228517-2008-076.

2. Louis DN, Ohgaki H, Wiestler OD, Cavenee WK, Burger PC, Jouvet A, Scheithauer BW, Kleihues P. The 2007 WHO Classification of Tumours of the Central Nervous System. Acta Neuropathol. 2007;114(2):97-109. doi:10.1007/s00401-007-0243-4.

3. Louis DN, Perry A, Wesseling P, Brat DJ, Cree IA, Figarella-Branger D, et al. The 2021 WHO Classification of Tumors of the Central Nervous System: A Summary. Neuro-Oncology. 2021;23(8):1231-51. doi:10.1093/neuonc/noab106.

4. Kumar V, Fausto N, Abbas A. Robbins and Cotran Pathologic Basis of Disease, 7th Ed. Elsevier Saunders, Philadelphia, 2005.

5. Rees J, Smirniotopoulos J, Jones R, Wong K. Glioblastoma Multiforme: Radiologic-Pathologic Correlation. Radiographics. 1996;16(6):1413-38; quiz 1462. doi:10.1148/radiographics.16.6.8946545.

6. Siegel RL, Miller KD, Jemal A. 2015 Cancer statistics. CA Cancer J Clin. 2015;65(1):5–29. doi: 10.3322/caac.21254.

7. Hanif F, Muzaffar K, Perveen K, Malhi SM, Simjee ShU. Glioblastoma Multiforme: A Review of its Epidemiology and Pathogenesis through Clinical Presentation and Treatment. Asian Pac J Cancer Prev. 2017;18(1):3-9. doi: 10.22034/APJCP.2017.18.1.3.

8. Smoll N R, Schaller K, Gautschi OP. Long-term survival of patients with glioblastoma multiforme (GBM). J Clin Neurosci. 2013;20(2):670–5. doi: 10.1016/j.jocn.2012.05.040.

9. Garcia-Alloza M, Bacskai BJ. Techniques for brain imaging in vivo. Neuromol Med. 2004;6:65–78. doi: 10.1385/nmm:6:1:065.

10. Pichlmeier U, Bink A, Schackert G, Stummer W, ALA Glioma Study Group. Resection and survival in glioblastoma multiforme: an RTOG recursive partitioning analysis of ALA study patients. Neuro Oncol. 2008;10(6):1025–1034. doi: 10.1215/15228517-2008-052.

11. Yates LR, Seoane J, Le Tourneau C, Siu LL, Marais R, Michiels S, et al. The European Society for Medical Oncology (ESMO) precision medicine glossary. Ann Oncol. 2018;29:30–5. doi: 10.1093/annonc/mdx707.

12. Vogelstein B, Papadopoulos N, Velculescu VE, Zhou S, Diaz LA, Jr, Kinzler KW. Cancer genome landscapes. Science. 2013;339:1546–1558. doi: 10.1126/science.1235122.

13. Patel SP, Schwaederle M, Daniels GA, Fanta PT, Schwab RB, Shimabukuro KA, et al. Molecular inimitability amongst tumors: implications for precision cancer medicine in the age of personalized oncology. Oncotarget. 2015;6:32602–32609. doi: 10.18632/oncotarget.5289.

14. Pena GP, de Andrade-Filho JS. How does a pathologist make a diagnosis? Arch Pathol Lab Med. 2009;133:124–132. doi: 10.5858/133.1.124.

15. Liu Y, Xu J. High-Resolution Microscopy for Imaging Cancer Pathobiology. Curr Pathobiol Rep 2019;7:85–96. https://doi.org/10.1007/s40139-019-00201-w.

16. Oh BH, Kim KH, Chung KY. Skin imaging using ultrasound imaging, optical coherence tomography, confocal microscopy, and two-photon microscopy in cutaneous oncology. Front Med. 2019;6:274. doi: 10.3389/fmed.2019.00274.

17. Mogensen M, Thrane L, Jørgensen TM, Andersen PE, Jemec GBE. OCT imaging of skin cancer and other dermatological diseases. J Biophoton. 2009;2:442–451. doi: 10.1002/jbio.200910020.

18. González S, Sánchez V, González-Rodríguez A, Parrado C, Ullrich M. Confocal microscopy patterns in nonmelanoma skin cancer and clinical applications. Actas Dermosifiliogr. 2014;105:446–58. doi: 10.1016/j.adengl.2014.04.007.

19. Zipfel WR, Williams RM, Christie R, Nikitin AY, Hyman BT, Webb WW. Live tissue intrinsic emission microscopy using multiphoton-excited native fluorescence and second harmonic generation Proc Natl Acad Sci. 2003;100 7075–80. doi:10.1073/pnas.0832308100

20. Radu Hristu, Lucian G Eftimie, Stefan G Stanciu, Remus R Glogojeanu, Pavel Gheorghita, George A Stanciu. Assessment of Extramammary Paget Disease by Two-Photon Microscopy. Front Med (Lausanne). 2022 Feb 25;9:839786. doi: 10.3389/fmed.2022.839786.

21. Enache A, Eftimie LG, Graur AM, Glogojeanu RR, Geambaşu A, Voinea OC, et al. Assessment of Cerebral Tumors and Metastases by Two-Photon Excitation Microscopy. Rom J Military Med. 2023;CXXVI(4):418-423. https://doi.org/10.55453/rjmm.2023.126.4.11.

22. Zhuo SM, Yan J, Chen G, Chen JX, Liu YC, Lu JP, et al. Label-free monitoring of colonic cancer progression using multiphoton microscopy. Biomed Opt Express. 2011;2(3):615–9. doi:10.1364/BOE.2.000615.

23. Mostany R, Miquelajauregui A, Shtrahman M, Portera-Cailliau C. Two-photon excitation microscopy and its applications in neuroscience.In: Verveer, P. (eds), Advanced Fluorescence Microscopy. Methods in Molecular Biology, vol 1251. Humana Press, 2015, New York, NY. https://doi.org/10.1007/978-1-4939-2080-8_2 2015.

24. Madden KS, Zettel ML, Majewska AK, Brown EB. Brain tumor imaging: live imaging of glioma by two-photon microscopy. Cold Spring Harb Protoc. 2013;2013(3):pdb.prot073668. doi: 10.1101/pdb.prot073668.

25. Ricard C, Stanchi F, Rodriguez T, Amoureux M C, Rougon G, Debarbieux F. Dynamic quantitative intravital imaging of glioblastoma progression reveals a lack of correlation between tumor growth and blood vessel density PLoS One 2013;8(9):e72655. doi: 10.1371/journal.pone.0072655.

26. Ricard C, Stanchi F, Rougon G, Debarbieux F. An orthotopic glioblastoma mouse model maintaining brain parenchymal physical constraints and suitable for intravital two-photon microscopy. J Vis Exp. 2014;86:51108. doi: 10.3791/51108.

27. Qin Y, Xia Y. Simultaneous two-photon fluorescence microscopy of NADH and FAD using pixel-to-pixel wavelength-switching. Front Phys. 2021;9:642302. doi: 10.3389/fphy.2021.642302.

28. Helmchen F. Two-photon functional imaging of neuronal activity.In: Frostig RD (ed.), In Vivo Optical Imaging of Brain Function. 2nd edition. Boca Raton, Florida, CRC Press/Taylor&Francis, 2009.

29. Liang W, Chen D, Guan H, Park HC, Li K, Li A, et al. Label-free metabolic imaging in vivo by two-photon fluorescence lifetime endomicroscopy. ACS Photonics 2022;9(12):4017-4029. doi: 10.1021/acsphotonics.2c01493.

30. Benninger RKP, Piston DW. Two-photon excitation microscopy for the study of living cells and tissues. Curr Protoc Cell Biol. 2013 Jun;Chapter 4:4.11.1-4.11.24. doi: 10.1002/0471143030.cb0411s59.

31. Zipfel WR, Williams RM, Webb WW. Nonlinear magic: multiphoton microscopy in the biosciences. Nature Biotechnology 2003;21(11):1369–1377. doi: 10.1038/nbt899.

32. Zhang Y, Chen Y, Yu Y, Xue X, Tuchin VV, Zhu D. Visible and near-infrared spectroscopy for distinguishing malignant tumor tissue from benign tumor and normal breast tissues in vitro. Journal of Biomedical Optics. 2013;18(7):077003. doi: 10.1117/1.JBO.18.7.077003.

33. Skala MC, Riching KM, Bird DK, Gendron-Fitzpatrick A, Eickhoff J, Eliceiri KW, et al. In vivo multiphoton fluorescence lifetime imaging of protein-bound and free NADH in normal and pre-cancerous epithelia. Journal of Biomedical Optics. 2007;12(2):024014. doi:10.1117/1.2717503.

34. Ostrander JH, McMahon CM, Lem S, Millon SR, Brown JQ, Seewaldt VL, Ramanujam N. Optical redox ratio differentiates breast cancer cell lines based on estrogen receptor status. Cancer Research. 2010;70(11):4759-4766. DOI: 10.1158/0008-5472.CAN-09-2572.

35. Campagnola P. Second harmonic generation imaging microscopy: applications to diseases diagnostics. Analytical Chemistry. 2011;83(9):3224-3231. doi: 10.1021/ac1032325.

36. Mertz J. Nonlinear microscopy: new techniques and applications. Current Opinion Neurobiology. 2004;14(5):610-616. doi: 10.1016/j.conb.2004.08.013.